ISSN 1054-660X, Laser Physics, 2011, Vol. 21, No. 7, pp. 1230–1234.

Laser-Induced Hydrodynamics in Water-Saturated Biotissues: 2. Effect on Delivery Fiber

V. I. Yusupov[a, b, *], V. M. Chudnovskii[a], and V. N. Bagratashvili[b]

[a] *Il'ichev Pacific Oceanological Institute, Far Eastern Branch, Russian Academy of Sciences, 43 Baltiyskaya str., Vladivostok, 690041Russia*

[b] *Institute on Laser and Information Technologies, Russian Academy of Sciences, 2 Pionerskaya str., Troitsk, Moscow oblast, 142190 Russia*

*e-mail: iouss@yandex.ru

Received January 19, 2011; in final form, January 26, 2011

Abstract—The degradation of the end surface of the delivery fiber due to the laser-induced hydrodynamic processes caused by the irradiation of the water-saturated tissue by CW laser with a wavelength of 970 nm and moderate power (1–10 W) is analyzed. It is demonstrated that the temperature in the vicinity of the end surface can be up to several thousand degrees at a laser intensity of about 10^4 W/cm^2. Relatively high temperatures and pressures that are reached upon the collapse of the cavitation microbubbles lead to the formation of the nanosized diamond-phase particles and supercritical water, which also facilitates the degradation of fiber.

DOI: 10.1134/S1054660X11140015

INTRODUCTION

The laser-induced hydrodynamic processes that take place when the moderate-power (1–10 W) laser radiation is delivered via the optical fiber to the water-saturated biotissues [1–3] are significant for several new approaches to the laser treatment of the diseases of connective tissues in cartilages, joints, and vertebral column [4–8]. The recently developed technologies for the treatment of osteochondrosis [5–7] and osteomyelitis [8] are based on the formation of channels in tissues using the heating of the quartz fiber with the carbon-coated (blackened) end surface by the laser radiation with a wavelength of 970 nm and a power of 3 W. Such an approach allows a significant increase in the heating rate of biotissues in the vicinity of the fiber end and the fast formation of channels in biotissues [6–8]. In previous work [1], we studied the biologically important hydrodynamic effects in water (in particular, the generation of vapor bubbles) induced by the moderate-power laser radiation with a wavelength of 970 nm in the vicinity of the heated blackened end surface of fiber. It was shown that intense hydrodynamic processes originate in liquid in the vicinity of the blackened end surface (fiber tip). They are caused by fast heating of end surface followed by explosive boiling of water. The diameters of the resulting bubbles range from a few microns to several tens of microns, and the velocities of the bubbles in the vicinity of the end surface of the fiber amount to 100 mm/s. Note also the possibility of stable bubble microjets. The generation of bubbles in the capillary that mimics the laser channel in biotissues leads to the formation of stable circulating flows with periods ranging from 0.2 to 1.0 s. The experiments show that such hydrodynamic effects can lead to the significant degradation of the distal end of delivery fiber. The laser-induced damage of the distal end of fiber is well known in the practical medical technologies using high-power Nd:YAG, alexandrite, and dye lasers with pulse durations of less than 1 μs and peak intensities of greater than 10^8 W/cm^2 [9–11]. The fiber is destroyed due to the effect of shock waves that result from the plasma formation, rapid thermal expansion, or collapse of cavitation bubbles [12–14]. The destruction of the optical fiber whose end surface is immersed in water results from the action of the holmium-laser radiation with a pulse duration of 200–350 μs at significantly lower peak intensities (about 10^7 W/cm^2) [15]. In this case, the destruction of fiber is caused by the cavitation collapse of vapor bubbles that emerge in the vicinity of the end surface of the fiber due to the effective absorption of the laser radiation. Note the absence of data on the degradation of fiber under the action of the moderate-power CW laser radiation, which is widely used in the modern laser medicine [4–8] at intensities of about 10^4 W/cm^2. Evidently, such processes must be taken into account owing to the significant effect on the irradiation parameters and the results of the laser action on biotissues. In addition, the analysis of the action of the laser-induced hydrodynamics on the delivery fiber can be used for the interpretation of the complicated processes that occur in the vicinity of the fiber end surface upon puncturing of water-saturated biotissues [1–3, 16].

In this work, we study the degradation of the end surface of delivery fiber using the moderate-power (1–10 W) laser radiation with a wavelength of 970 nm and consider possible scenarios of such processes.

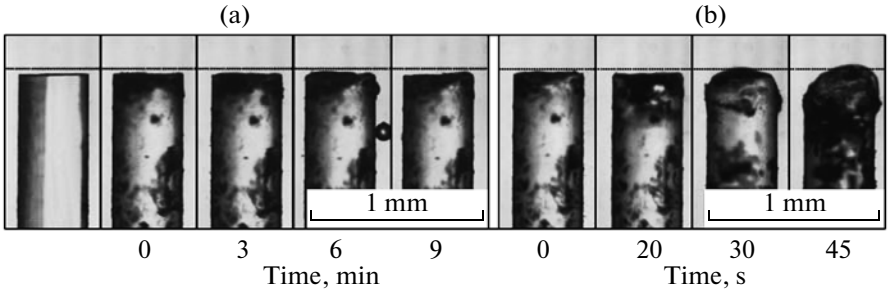

Fig. 1. Modifications of the profile of the blackened end surface (side view) for the two regimes of the laser action and several irradiation times: (a) stationary regime (the fiber is immersed in water, the left-hand panel shows the original fiber, and the laser power is 3 W) and (b) regime of channel formation (the channel is formed by the fiber that moves inside the wooden bar and the radiation power is 5 W).

MATERIALS AND METHODS

We study the laser-induced hydrodynamic effects with the aid of the optical methods using the Plexiglas cell filled with water. The horizontal dimensions of the cell are 150 × 100 mm, and the height is 15 mm. An IRE-Polyus LS-0.97 fiber laser with an output power of 0–10 W and a wavelength of 970 nm is interfaced with a quartz delivery fiber with a diameter of 400 μm and serves as the radiation source. The working end of the delivery fiber is preliminary blackened using a short (about 1 s) contact with a wooden bar at a laser power of about 3 W [1]. In the experiments, we employ two regimes that are widely used in medical practice [4–8]: (i) stationary regime with fixed fiber and (ii) regime of channel formation in which a wooden bar that mimics the biotissue is pressed to the heated end surface in water over 3 s (the fiber burns a channel in the bar and is shifted inside the bar by several millimeters).

The cell with the fixed fiber is placed on the worktable of a MICROS MC300 microscope (Austria), which is equipped with a Vision color video camera. We measure the temperature in the vicinity of the fiber end surface in the regime of the channel formation using an optical pyrometer based on an Ocean Optics USB4000 (USA) fiber spectrum analyzer. The measurement fiber of the pyrometer is placed in the immediate vicinity of the end surface of the delivery fiber, so that the optical radiation resulting from the heating of the sample that mimics the biotissue is effectively collected at the distances 50–500 μm from the end surface. We study the end surface of the delivery fiber using a LEO 1450 scanning electron microscope (SEM, Germany) and a HORIBA Jobin Yvon T64000 (France) micro-Raman spectrometer.

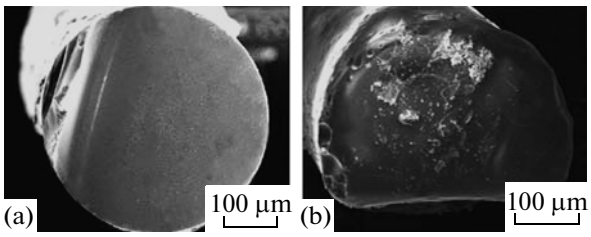

Fig. 2. SEM image of the working end surface of the optical fiber: (a) chipped end surface and (b) end surface resulting from the laser action in the regime of channel formation.

RESULTS AND DISCUSSION

The experiments show that the laser-induced processes that take place on the end surface of the laser fiber and in the vicinity of the end surface in water can substantially affect the end surface. Figure 1a demonstrates a series of photographs that show the modification of the profile of the working end surface for the stationary regime of the laser action on the blackened end surface in water at several irradiation times. It is seen that the modification of the end surface takes place: in particular, (edge) fragments of the end surface are etched.

More significant degradation of the end surface occurs in the regime of channel formation when the fiber is shifted inside the wooden bar that mimics the biotissue. In this case, we observe substantial modifications and the formation of the rounded end surface (Fig. 1b). The comparison of the sequential photographs yields a significant increase in the volume of the fiber fragment (swelling) in the vicinity of the working end surface.

The SEM images (Fig. 2) show that the laser action in the regime of the channel formation in the presence of water causes substantial modifications of the working surface: the sharp edge is rounded and surface irregularities (craters) emerge on the end surface. The magnified image (Fig. 3a) shows that a thin shell (film) with circular holes emerges on the end surface of the optical fiber. Multiple cracks pass through some of the holes. In addition, we observe elongated crystal-like structures on the surface (Fig. 3b). Looking through the largest hole in the film on the end surface (at the center of the lower part of the fragment in Fig. 3a),

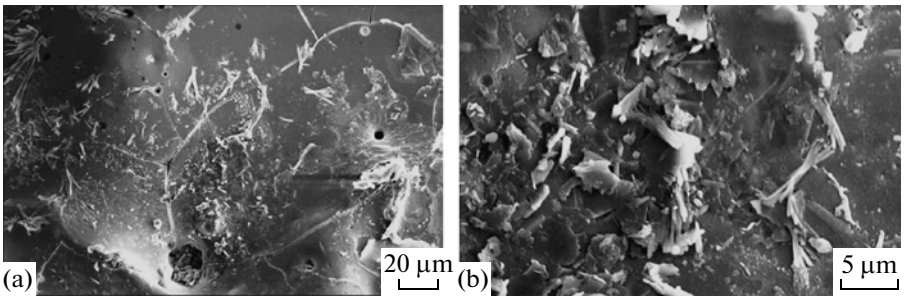

Fig. 3. Microstructure of the end surface of the delivery optical fiber after the laser action: (a) SEM image of a fragment of the fiber end surface and (b) magnified image of a fragment of the end surface with the crystal-like structures on the surface.

whose dimension in any direction is greater than 10 μm, we observe the inner micron-scale porous structure. Apparently, the formation of the porous structure due to the laser-induced hydrodynamic processes can be related to the swelling in the regime of the channel formation (Fig. 1b). Note that the 3D micron-scale irregularities can be effectively studied with the aid of the recently developed broadband digital holography [17].

We assume that the observed significant structural modifications of the fiber surface in the regime of the channel formation in the presence of water (Figs. 1–3) can be due to the fact that the temperature on the end surface becomes greater than the melting point of quartz (about 1700°C).

The temperature measurements in the vicinity of the fiber end using the optical pyrometry show that the temperature can be greater than the melting point of quartz (about 1700°C) at a laser power of 3–4 W and that the temperature significantly increases with a further increase in power. The pyrometric measurements show that a temperature of about 2600°C, which substantially exceeds the melting point of quartz, can be reached in the vicinity of the end surface of the delivery fiber at the above parameters. The heating to the temperatures that are significantly greater than the level of the thermal resistance of quartz glass (about 1200°C) (i.e., the minimum temperature at which the thermoelastic stress becomes greater than tensile strength of glass) must lead to the destruction of quartz in the vicinity of the end surface of delivery fiber. This can be the reason for the observed formation of the micron-scale porous structure (Fig. 3a), which leads to visible swelling of the fiber fragment in the vicinity of the end surface (Fig. 1b).

The typical micron-scale circular holes on the film surface (Fig. 3a) can be due to the cavitation collapse of single bubbles. It is well known that the cavitation collapse of the bubbles in liquid in the vicinity of the solid surface gives rise to the high-speed cumulative microjets that can destroy the solid surface [18, 19]. Apparently, this effect leads to multiple cracks on the film and the formation of the porous structure (Fig. 3), since the cumulative jets can punch holes, cause cracks in the film, and destroy the structure of the quartz fiber.

The collapse of the cavitation bubble leads to the generation of the high-pressure pulse, whose amplitude can be greater than 10^6 MPa [18] at a relatively low gas content, and causes the heating of the internal gas, so that the gas temperature rapidly increases to, at least, 10^4 K [18]. At such temperatures and pressures, we obtain the supercritical water (the critical pressure and temperature for water are $P_{cr} = 22.1$ MPa and $T_{cr} = 374$°C, respectively), which effectively dissolves the quartz glass [20]. Indeed, the modification of the fiber end surface (SEM image in Fig. 3a) is similar to the modification from [20] where the quartz fiber was etched in the supercritical water. Thus, the effect of the supercritical water that results from the laser heating of water in the vicinity of the blackened end surface must be also taken into account in the analysis of the degradation.

Figure 4 shows the Raman spectra of several fragments of the fiber end surface shown in Fig. 3. For comparison, we also present the typical spectral curves of graphite and diamond. Figure 4 shows that spectra *3–5*, which correspond to different fragments of the fiber end surface, exhibit two broad peaks, whose positions are close to the positions of the graphite Raman bands (curve *1*). However, as distinct from the spectrum of graphite, the peak amplitude in the interval 1300–1400 cm^{-1} is approximately equal to (curve *5*) or greater than (curves *3* and *4*) the peak amplitude in the interval 1540–1640 cm^{-1}. This can be due to the presence of the diamond crystals on the fiber end surface. The fact that the low-frequency bands in spectra *3–5* are wider than the Raman band of diamond peaked at 1330 cm^{-1} (curve *2*) can be due to the presence of the nanosized diamond particles [21, 22].

The reason for the synthesis of the diamond phase on the end surface of the laser fiber in the regime of the channel formation in the presence of water can be as follows. The intense hydrodynamic processes on the end surface and in the nearest vicinity [1] are accompanied by the explosive boiling and the formation of bubbles. In this case, the temperature and pressure can

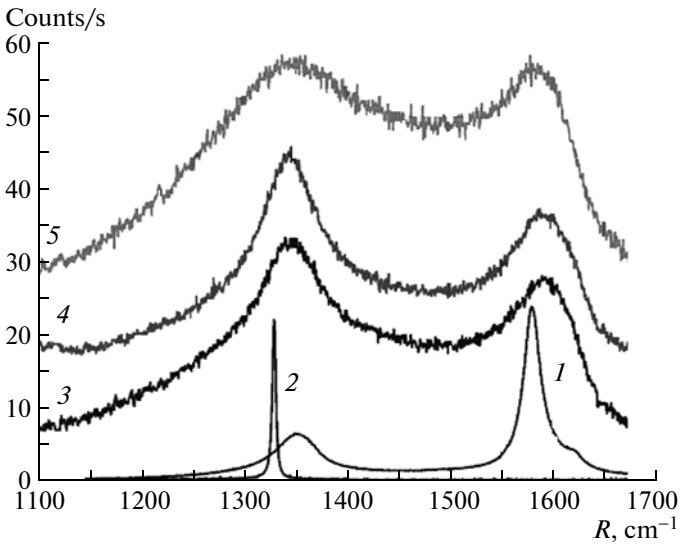

Fig. 4. Raman spectra of (*1*) graphite, (*2*) diamond, and (*3–5*) the fragments of the fiber end surface after the laser action in the regime of the channel formation.

be greater than the critical levels. In addition, the preliminary blackening with the burning of tissue in the vicinity of the heated end surface leads to the accumulation of carbon and, hence, the formation of the diamond nanoparticles. The experimental evidence in favor of the synthesis of the diamond phase upon the excitation of cavitation in the carbon-containing liquid can be found in [23]. The results from [24, 25] clearly show that the diamond nanoparticles are also formed when the cavitation is excited due to the action of laser pulses on a graphite substrate in water. The action of the high-intensity ultrasound on the carbon-containing liquid also leads to the formation of diamond nanoparticles [26]. Note that curve *4* in Fig. 5 almost coincides with the spectral curve for the 35-nm single diamond crystal from [27].

The nonuniformity of the action of the hydrodynamic processes on the end surface of the delivery fiber (Figs. 1–3) can be caused by the presence of specific spots that, in accordance with [1], are related to the thickness nonuniformity of the deposited carbon layer: the thicker the sample, the stronger the radiation absorption and, hence, the higher the temperature. At such spots, the rate of the bubble formation is higher, and the bubbles appear attached to such spots due to the additional heating with a decrease in the heat sink to water [1]. In addition, note the Marangoni effect [28]: the temperature gradient gives rise to the gradient of surface tension, which leads to the convective flows of liquid on the surface of the bubble and induces the force that presses the bubble to the hottest spot.

CONCLUSIONS

We study the action of the laser-induced hydrodynamic processes caused by the moderate-power CW laser radiation on the end surface of delivery fiber. It is demonstrated that the hydrodynamics caused by the laser heating in the free liquid volume can lead to the degradation of the fiber end surface over several minutes even at relatively low laser intensities (10^3–10^4 W/cm^2). The hydrodynamic processes in the regime of the channel formation result in more significant modifications over shorter times. In this regime, a channel is burnt by the laser-heated fiber end surface in the presence of water in a wooden bar that mimics the biotissue. Holes and cracks appear on the fused working surface, and the structure of the quartz fiber in the vicinity of the end surface appears damaged. Even at moderate laser powers and intensities of about 10^4 W/cm^2, the temperature in the vicinity of the end surface of delivery fiber can reach several thousand degrees. High temperatures and pressures resulting from the collapse of the cavitation microbubbles allow the growth of a new phase (nanosized diamonds) and the formation of the supercritical water, which also facilitates the degradation of fiber. The observed significant degradation of the delivery fiber due to multiple irregularities of different scales causes substantial modification of the irradiation of biotissues [29, 30].

Finally, note that the above laser-induced hydrodynamic effects are accompanied by high-intensity acoustic signals in a wide frequency range (up to 10 MHz [18, 31] and even greater [32]). The analysis of the optoacoustic effects related to the laser-induced hydrodynamic processes that occur in the vicinity of the fiber end surface upon the laser action on the water-saturated tissues will be presented in the next work of the series.

ACKNOWLEDGMENTS

This work was supported by the Russian Foundation for Basic Research (project no. 09-02-00714).

REFERENCES

1. V. I. Yusupov, V. M. Chudnovskii, and V. N. Bagratashvili, Laser Phys. **20**, 1641 (2010).
2. V. Chudnovskii, V. Bulanov, and V. Yusupov, Photonics **1**, 30 (2010).
3. V. M. Chudnovskii, V. A. Bulanov, V. I. Yusupov, V. I. Korskov, and V. S. Timoshenko, Laser Med. **14**, 30 (2010).
4. *Laser Engineering of Cartilages*, Ed. by V. N. Bagratashvili, E. N. Sobol, and A. B. Shekhter (Fizmatlit, Moscow, 2006) [in Russian].
5. B. I. Sandler, L. N. Sulyandziga, V. M. Chudnovskii, V. I. Yusupov, O. V. Kosareva, and V. C. Timoshenko, *Prospects for Treatment of Discogenic Compression Forms of Lumbosacral Radiculitis Using Puncture Nonendoscopic Laser Surgery* (Dalnauka, Vladivostok, 2004) [in Russian].
6. B. I. Sandler, L. N. Sulyandziga, V. M. Chudnovskii, V. I. Yusupov, and Y. M. Galin, Bull. Physiol. Pathol. Breath **11**, 46 (2002).
7. V. M. Chudnovskii, and V. I. Yusupov, "Method of Laser Intervention Effects in Osteochondrosis," Patent RF No. 2321373, Byull. Izobret. No. 10 (2008).
8. V. A. Privalov, I. V. Krochek, and A. V. Lappa, SPIE Proc. **4433**, 180 (2001).
9. K. Rink, G. Delacretaz, and R. P. Salathe, Laser Surg Med. **16**, 134 (1995).
10. *Laser Surgery: Advanced Characterization, Therapeutics, and Systems II*, Ed. by S. N. Joffe and K. Atsumi, Proc. SPIE, Vol. 1200 (Los Angeles, 1990).
11. C. Strunge, R. Brinkmann, G. Flemming, and R. Engelhardt, Laser Surg. Med. **11**, 183 (1991).
12. K. Rink, G. Delacretaz, and R. P. Salathe, Appl. Phys. Lett. **61**, 2644 (1992).
13. K. Rink, G. Delacretaz, and R. P. Salathe, Appl. Phys. Lett. **61**, 258 (1992).
14. T. Asshauer, K. Rink, and G. Delacr'etaz, J. Appl. Phys. **76**, 5007 (1994).
15. T. Asshauer and G. Delacretaz, Laser Med. Sci. **12**, 157 (1997).
16. E. Sobol, O. Zakharkina, A. Baskov, A. Shekhter, I. Borschenko, A. Guller, V. Baskov, A. Omelchenko, and A. Sviridov, Laser Phys. **19**, 825 (2009).
17. D. V. Shabanov, G. V. Geliknov, and V. M. Gelikonov, Laser Phys. Lett. **6**, 753 (2009).
18. M. Sirotyuk, *Acoustic Cavitation* (Nauka, Moscow, 2008) [in Russian].
19. S. Kenneth, *The Chemistry of Ultrasound* (Suslick. Enc. Brit., Chicago, 1994).
20. V. N. Bagratashvili, A. N. Konovalov, A. A. Novitskiy, M. Poliakoff, and S. I. Tsypina, Russ. J. Phys. Chem. B **3**, 1154 (2009).
21. J. Schwan, S. Ulrich, V. Batori, and H. Ehrhardt, J. Appl. Phys. **80**, 440 (1996).
22. D. S. Knight and W. B. J. Mater. Res. **4**, 385 (1989).
23. E. M. Galimov, A. M. Kudin, V. N. Skorobogatsky, V. G. Plotnichenko, O. L. Bondarev, B. G. Zarubin, V. V. Strazdovsky, A. S. Aronin, A. V. Fisenko, I. V. Bykov, and A. Y. Barinov, Dokl. Akad. Nauk **395**, 187 (2004) [Dokl. Phys. **49**, 150 (2004)].
24. S. R. J. Pearce, S. J. Henley, F. Claeyssens, P. W. May, K. R. Hallam, J. A. Smith, and K. N. Rossera, Diam. Relat. Mater. **13**, 661 (2004).
25. L. Yang, P. W. May, L. Yinb, J. A. Smith, and K. N. Rosser, Diam. Relat. Mater. **16**, 725 (2007).
26. A. Kh. Khachatryan, S. G. Aloyan, P. W. May, R. Sargsyan, V. A. Khachatryan, and V. S. Baghdasaryan, Diam. Relat. Mater. **17**, 931 (2008).
27. K. W. Sun, J. Y. Wang, and T. Y. Ko, J. Nanopart. Res. **10**, 115 (2008).
28. D. W. Berry, N. R. Heckenberg, and H. Rubinszteindunlop, J. Mod. Opt. **47**, 1575 (2000).
29. E. E. Gorodnichev, A. I. Kuzovlev, and D. B. Rogozkin, Laser Phys. **20**, 1961 (2010).
30. S. D. Campbell, T. P. Garvin, I. L. Goodin, Q. Su, and R. Grobe, Laser Phys. **19**, 238 (2009).
31. I. M. Pelivanov, D. S. Kopylova, N. B. Podymova, and A. A. Karabutov, Laser Phys. **19**, 1350 (2009).
32. A. A. Samokhin, V. I. Vovchenko, N. N. Il'ichev, and P. V. Shapkin, Laser Phys. **19**, 1187 (2009).